Appl. Phys. A (2015) 120:1427–1434
DOI 10.1007/s00339-015-9329-3

Applied Physics A
Materials Science & Processing

Effect of copper oxide on structure and physical properties of lithium lead borate glasses

I. Kashif[1] · A. Ratep[2]

Received: 11 February 2015 / Accepted: 30 June 2015 / Published online: 10 July 2015

Abstract Copper-doped Lead lithium borate glass samples with the composition of (35-x) Pb_3O_4–xCuO–65$Li_2B_4O_7$, where $x = 5$, 10, 15 or 20 mol%, have been prepared by melt quenching technique. Glass-forming ability, density, electrical conductivity, magnetic susceptibility and structural properties of lead lithium borate glasses have been investigated. IR spectroscopic data show that the copper ions play the role of glass modifier. Addition of CuO influences $BO_3 \leftrightarrow BO_4$ conversion. Density is expressed in terms of the structural modifications that take place in glass matrix. The increase in Tg reflects an increase in bond strength, and samples obtain more rigid glass structure. Electrical conductivity and magnetic susceptibility χ data show a variable behavior with the increase in the copper content in two valance states Cu^{+} and Cu^{+2}. In addition, optical properties depend on the change of the role of copper ions in the samples' structure. Optical energy band gap E_{opt} and Urbach energy E_{tail} are determined. The increase in E_{opt} and UV cutoff with an increase in CuO content is due to the decrease in non-bridging oxygen concentration. The decrease in E_{tail} at higher concentrations is attributed to the copper ion accumulation in the interstitial positions and to the formation of orthoborate groups. These samples are suitable for the green light longpass filters.

✉ I. Kashif
ismailkashif52@yahoo.com

[1] Physics Department, Faculty of Science, Al-azhar University, Nasrcity, Cairo 11884, Egypt

[2] Physics Department, Faculty of women, Ain Shams University, Heliopolis, Cairo, Egypt

1 Introduction

The study of the structures of glasses is necessary to obtain a good understanding of structure–property relations. Boron atoms in lithium borate glasses are either three- or four-coordinated and are generally designed as BO_3 and BO_4 units. The presence of BO_4 units leads to the tetrahedral network of the glass [1].

The effect of copper addition on lithium borate glass samples was studied: The copper ions can act as network modifier and some ions as network former by increasing the copper content. The magnetic, electrical and optical properties show a variable behavior due to the presence of copper ions in two valances, cuprous (Cu^{+}) and cupric (Cu^{2+}), in glass samples [2]. In our study, lithium borate glass containing lead was studied. The results showed the presence of lead oxide lowering the average coordination number of oxygen [3]. This causes the increase in refractive index and density.

The structure of PbO–B_2O_3 glasses containing 10–80 mol% PbO was investigated. The structure studies revealed that the PbO content varied between 10 and 20 mol% and PbO acts as a network modifier. With the increase in PbO content, the borate group changed from [BO_3] to [BO_4] units. When the content is over 60 mol%, PbO plays the role of glass former. Four possible structure models have been suggested to explain the effects of PbO on glass network [4]:

1. Three-coordinated boroxol rings modified by Pb^{2+};
2. Formation of Pb–O–B covalent bonds;
3. Bridge networks between [BO_3] and [BO_4] units;
4. Complex structures of Pb^{2+}-modified boron oxygen rings and chains.

In this work, we study the effect of substitution of Pb_3O_4 with CuO in lithium lead borate glass system on structure, electrical, magnetic and optical properties.

2 Experimental work

A series of lithium lead borate glass samples containing CuO were prepared. The details of the compositions chosen for the present study are given in Table 1. The homogenous mixture was melted in a platinum crucible in an electrically programmable heated furnace, (type UAF 15/10 Lenton Thermal Designs), equipped with an automatic temperature controller. The samples were melted at 1200 ± 20 °C for 2 h with a heating rate of 30 °C/min. The molten materials were stirred several times to ensure complete homogeneity. Then, they were quenched in air and poured at room temperature between two Cu plates.

The samples were examined using a Philips Analytical X-ray diffraction system, type PW 3710 with Cu tube anode. It can be seen that all samples are in a glassy state. FTIR spectra were recorded with a FTIR spectrometer (type JASCO FT/IR-430, Japan) in the wave number range 220–2000 cm^{-1} at room temperature by using the KBr disc technique. Differential scanning calorimetric measurements (DSC) were taken using a SHIMADZU DTA-50 analyzer. The measurements were taken between 25 and 650 °C (in air using Al_2O_3 powder as a reference material) at the rate of 35 °C/min.

The density of glasses was determined by Archimedes method in which glass sample was weighed three times in air and when immersed in toluene at 25 °C. The density was calculated from the formula

$$\rho = [W_a/(W_a - W_b)] \times 0.8635$$

where ρ is the density of the glass sample, W_a is the weight of the glass sample in air, W_b is the weight of the glass sample in toluene and 0.8635 is the density of toluene.

For good electrical contact during measurements, the sample surfaces were highly polished and coated with an air-drying silver paste. The electrical conductivity measurements at room temperature were obtained with a programmable Keithley electrometer (type 617). Magnetic susceptibility was measured by applying Gouy method using a Faraday electromagnet. Optical absorption measurements were carried out using ***V 570 JASCO*** spectrophotometer.

Table 1 Glass samples' composition (mol%)

Sample no.	$Li_2B_4O_7$	Pb_3O_4	CuO
1	65	35	–
2	65	30	5
3	65	25	10
4	65	20	15
5	65	15	20

3 Results and discussion

The X-ray diffraction patterns of the [65 mol% $Li_2B_4O_7$-(35-x) mol% Pb_3O_4-x mol% CuO] glass samples (x = 0, 5, 10, 15 or 20 mol%) are shown in Fig. 1. All the samples show broad halo around a diffraction angle 2θ = 32°, characteristic of an amorphous structure and confirming the absence of crystal in the samples.

The density is related to how the modifier and former ions groups are packed together in the structure. Figure 2 shows the relation between the density and copper content. From Fig. 2, it can be observed that the density decreases with the increase in Cu content. Substitution of Pb (having high molecular weight) with Cu (having low molecular weight) decreases the density. Density is directly proportional to the molecular weight, and the increase in Cu content decreases the formation of tetrahedral groups (BO_4), and increasing the triangle groups (BO_3) led to the increase in borate non-bridging oxygen (NBO) [5], increasing volume which is inversely proportional to the density.

Density plays an essential role in calculating the concentration of ions added, polaron radius and the time between additions of ions. In the glass samples under study, the concentration of copper ions per unit volume can be calculated using the equation [6]:

$$N = \rho\, \mathrm{Na}/100\, W\ \mathrm{cm}^{-1}$$

where ρ is the density of glass sample, Na is the Avogadro's number and W is the atomic weight of copper in the

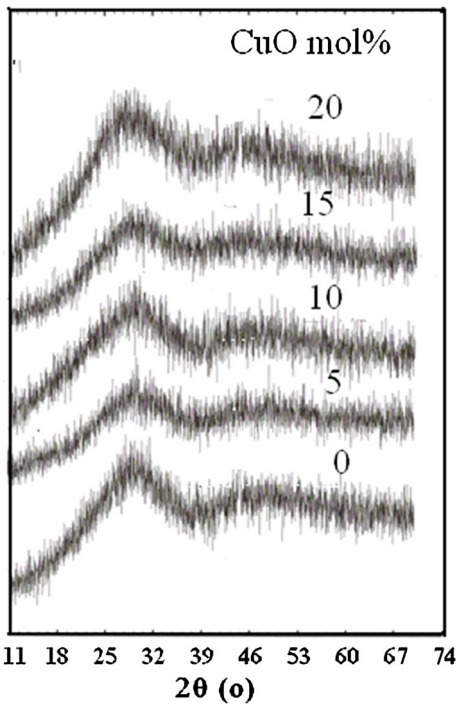

Fig. 1 X-ray diffraction patterns of the glass samples

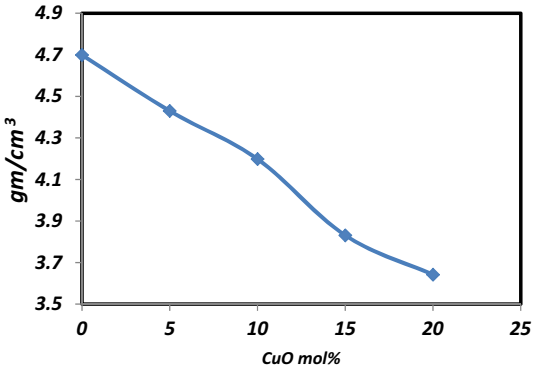

Fig. 2 Relation between the density and copper oxide content

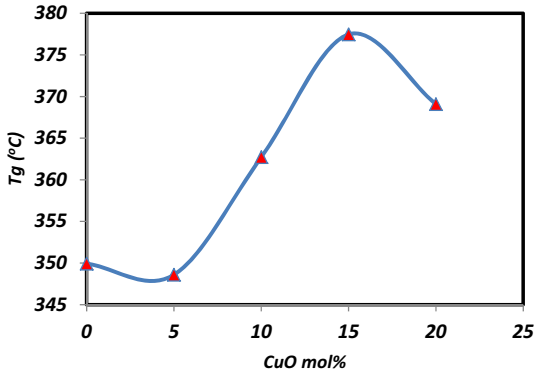

Fig. 3 Relation between the glass transition temperature and the Cu content

glass sample. From the calculated values of N, the polaron radius (r_p) can be determined using the relation:

$$r_p = 0.5\,(\pi/6N)^{1/3}\text{cm}$$

Also, the space between Cu–Cu atoms in the glass system can be calculated from the values of N from the equation:

$$R = (1/N)^{1/3}\text{cm}$$

All the calculated parameters of N, r_p and R are shown in Table 2.

From these results, it can be concluded that the separation between Cu–Cu (R) is greater than polaron radius (r_p) for all samples. And the values of r_p are smaller than R and greater than the ionic radius of copper (ionic radius of Cu ion is 0.74E-12 cm), which indicates that electrons are localized [6].

In the thermal studies using DTA, the appearance of single peak due to the glass transition temperature of all glass samples indicates the high homogeneity of the glass prepared [5, 7]. Figure 3 indicates the relation between the glass transition temperature and the Cu content. From Fig. 3, it can be observed that the value of Tg increases with Cu content up to 15 mol% and then decreases.

The glass transition temperature depends on the glass structure, and glass transition is related to the density of covalent cross-linking, the oxygen density of the network and the number and strength of the cross-links between oxygen and the cation [8, 9].

Table 2 Concentration of copper ions per unit volume N, the polaron radius (r_p) and the space between Cu–Cu atoms R

CuO (mol%)	N (cm^{-3})	R_P (cm)	R (cm)
5	7.24 E21	2.08E-8	5.17E-8
10	1.37 E22	1.68E-8	4.18E-8
15	1.92 E22	1.50E-8	3.74E-8
20	2.39 E22	1.39E-8	3.47E-8

In the glass samples, the substitution of Pb by Cu decrease the oxygen density which led to the compactness of the structure and increasing the glass transition temperature up to 15 mol% and then decrease, the decrease in the value of Tg as between $10 < \text{PbO} < 20$ mol%, shows that the Pb ions act as a network modifier [4].

The temperature difference between the crystallization temperature Tc and transition temperature Tg reflects the glass-forming ability (GFA) and is expressed by $\Delta Tc = Tc - Tg$, which is called the width of the supercooled liquid region (SCL). ΔTc is a good indication of thermal stability because the higher the value of this difference, the more is the delay in the nucleation process [10].

Figure 4 shows the glass-forming ability as a function of copper oxide content. From Fig. 4, it can be observed that $\Delta Tc = Tc - Tg$ increases with the addition of copper oxide content up to 10 mol% and then decreases. A large value of ΔTc at 10 mol% CuO implies that the supercooled liquid can exist in a wide temperature range without crystallization and has a resistance to the nucleation and growth of crystallization phases, leading to good GFA and then decreasing with increasing CuO content.

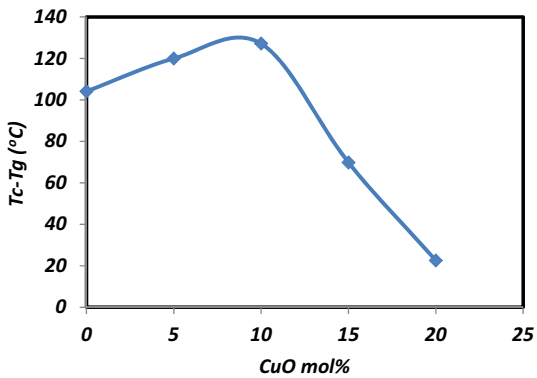

Fig. 4 Glass-forming ability as a function of copper oxide content

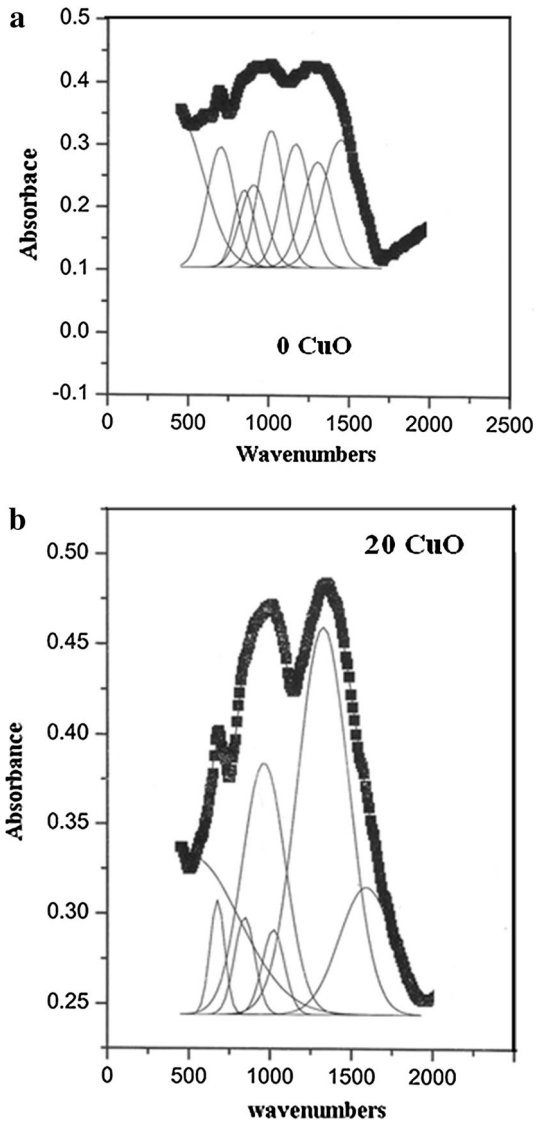

Fig. 5 FTIR spectra of the glass samples free from copper and samples containing 20 mol% CuO

Figure 5 shows the FTIR spectra of the glass samples free from copper and samples containing 20 mol% CuO.

From Fig. 5 (the spectrum of the sample free from CuO), it can be observed that the fundamental absorption bands are at 1450, 1300, 1165, 1015, 900, 850, 700 and 430 cm^{-1}. The band at 1450 cm^{-1} attributed to triangle boron oxygen triangle groups [11] while the band at 1356 cm^{-1} is due to asymmetric stretching modes of borate triangles $B\emptyset_3$ and $B\emptyset_2O$ (Ø representing an oxygen atom bridging two boron atoms and O-NBO) [12] various borate rings. The band at 1165 cm^{-1} is due to the B–O stretching modes of borate triangles BO_3 [13]. The band at 1038 cm^{-1} is due to the vibration of BO_4 tetrahedra, which is present as pentaborate, tetraborate, diborate and triborate groups [4, 14]. The band at 950 cm^{-1} is attributed to Pb–O bonds [15].

The band at 840 cm^{-1} is due to the pentaborate, diborate and triborate vibrations. The band at 700 cm^{-1} results from oxygen bridges forming between one tetrahedral and one trigonal boron atom [2]. Moreover, the band at 620 cm^{-1} is the characteristic of the vibration frequency of lead [16].

The replacement of PbO by CuO causes a decrease in the intensity of bands at 620, 840, 1180, 1250 and 1356 cm^{-1}, which then disappear in sample containing 20 mol% CuO. This may occur due to the change in the network. No bands appear for Cu ions, and this indicates that the Cu ions act as network modifiers in this region of concentration.

From the relative peak areas of $\{B\acute{\emptyset}_3$ and $B\emptyset_2O–\}$ (A_3) and $\{B\emptyset_4–\}$ (A_4), which were separated by a Gaussian deconvolution, the value of $N4$ is calculated as $A_4/(A_4 + A_3)$. The quantities A_4 and A_3 reflect the relative content of tetrahedral ($B\emptyset_4$–) and triangular ($B\emptyset_3$ and $B\emptyset_2O$–) borate species, respectively (Ø representing an oxygen atom bridging two boron atoms).

The following method is used in the calculation of the fraction N_4 of the four-coordinated boron atoms in the glass, where [17]

$$N_4 = (\text{concentration of } BO_4 \text{ tetrahedral})/(\text{concentration of } BO_4 \text{ tetrahedral} + \text{concentration of } BO_3 \text{ triangle}) = A_4/(A_4 + A_3)$$

The obtained values are shown in Fig. 6 as a function of composition. N_4 decreases firstly with the addition of 5 mol% CuO. This decrease due to the decrease in the BO_4 groups with the replacement of lead oxide by copper oxide depends on the number of oxygen atoms, converts BO_4 to BO_3 and forms non-bridging oxygen. In addition, Pb ions act as former structure and Cu ions as network modifiers.

Figure 7 shows the relation between electrical conductivity and copper oxide content.

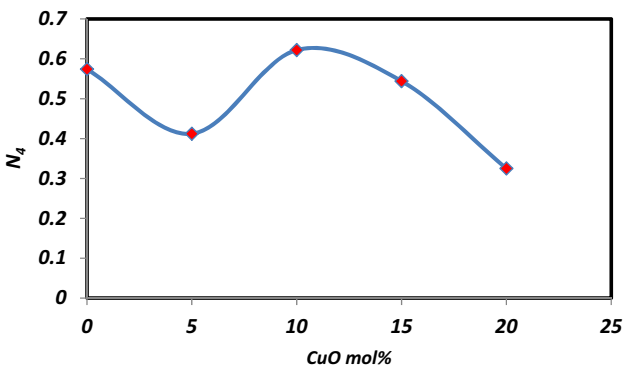

Fig. 6 Fraction N_4 of the four-coordinated boron atoms in the glass samples

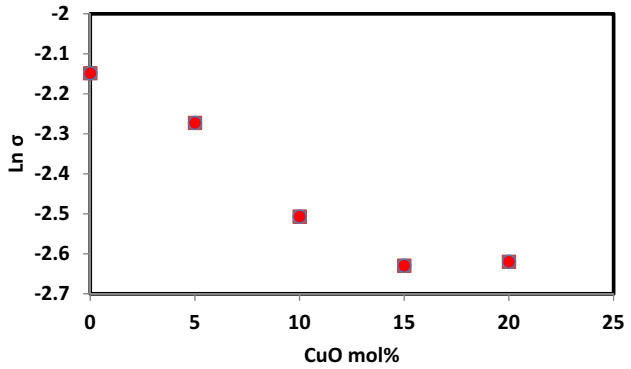

Fig. 7 Relation between the electrical conductivity and copper oxide content

From Fig. 7, it can be observed that the (Ln σ) decreases with the increase in the copper content. (Ln σ) decreases with the gradual increase in copper oxide content. The number of electron hopping processes in the glass network increases where the sample free from copper has the ionic conduction, although the conduction decreases with the increase in the copper content. In addition, as the number of Cu ions increases, they enter the interstitial vacancies to occupy the modifier positions replacing lead and at high concentration of copper occupy the network former and modifier positions.

Copper ions exist in two valance states, Cu^{+} and Cu^{+2} [18]. Electronic conduction occurs by polarons hopping between these two sites. Introduction of high ionic strength Cu in the form of CuO_6 instead of PbO_3 or PbO_4 decreases the conduction, and this reflects the change from ionic to mixed conduction [19].

Figure 8 shows the relation between the magnetic susceptibility and the concentration of CuO. It can be observed that the magnetic susceptibility increases with increasing Cu content up to 10 mol% and then decreases. The figure also shows a sudden decrease for sample containing CuO between 10 and 15 mol% and very slight

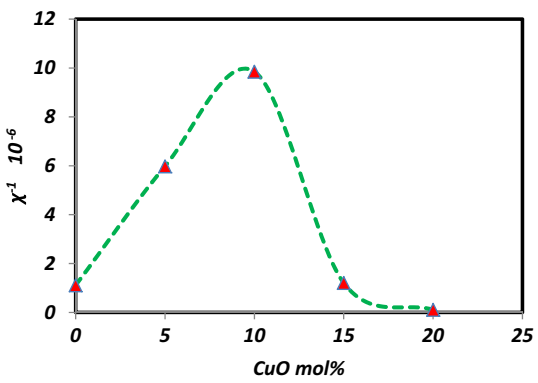

Fig. 8 Relation between the magnetic susceptibility and the concentration of CuO

decrease between 15 and 20 mol%. It is clear that the magnetic susceptibility χ depends on the change of the role of copper ions in the sample's structure due to the change in the copper glass-forming oxide [20]. In various glasses, Cu ions exist as Cu^{+}, Cu^{2+} and Cu^{o}, although most glasses melting under ordinary atmospheric conditions are usually assumed not to contain Cu^{o} [21–23]. The increase in the magnetic susceptibility χ by increasing the copper content up to 10 mol% CuO is attributed to the formation of Cu^{2+} ions, which have high magnetic moment (1.7 μ_B). By increasing the copper oxide content over 10 mol% CuO, the magnetic susceptibility χ decreases due to the conversion of Cu^{2+} ions to Cu^{+} ions, which have zero magnetic moment. The magnetic susceptibility χ showed stability in the glass samples having 15 mol% CuO and above. This may be because no more Cu^{2+} ions change to Cu^{+} ions, and this result is confirmed by electrical conduction results.

The visible absorption bands observed from the Cu-doped glass can be understood and related to the presence of Cu^{2+} ions. For the Cu^{2+} ion (d^9), the d–d transition can be considered [17].

Figure 9 shows the optical transmission of the glass samples. The cutoff for the UV and infrared is determined and tabulated in Table 1. From Fig. 9 can be observed that the glass samples has two absorption bands, one in the UV and the other in infrared except the free from copper have one absorption bands, in the UV. In addition, as the copper oxide increases, the infrared band shifts and the optical transmission of UV band decreases (Table 3).

The effect of copper oxide contents of the cutting bands in UV and IR due to the copper has two absorption bands, one in the UV and the other in infrared. Moreover, as copper oxide increases, the band shifts and the absorption UV band increases, until threshold contents of copper oxide begin to have a cutoff in infrared region.

Figure 10 shows the cutoff and bandstop filter of UV. These filters (glass sample) prevent the spectral lines' bandstop (UV). This filter, the UV bandstop, begins with 190 nm and increases with increasing the CuO doping; the UV cutoff, the end of the bandstop filter which starts from 350 to 460 nm, depends on the CuO concentration from 5

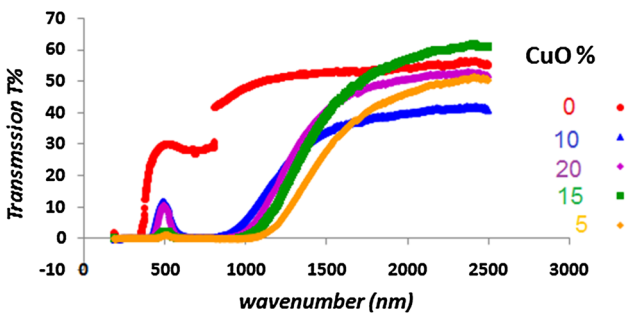

Fig. 9 Optical transmission of the glass samples

Table 3 UV and IR cutoff, bandstop, bandpass, band gap and band tail

CuO-Pb_3O_4 mol%	0–35	5–30	10–25	15–20	20–15
UV cutoff λ (nm)	350	400	425	450	460
UV bandstop λ (nm)	350–190	400–190	425–190	450–190	460–190
IR cutoff λ (nm)	–	700	650	600	570
IR bandstop λ (nm)	–	700–800	650–900	600–950	570–1060
Bandpass	–	400–700	425–650	450–600	460–570
Bandpass width	–	300	225	150	110
Bandpass HW	–	100	80	65	40
Bandpass center	–	490	495	500	510
Direct band gap (eV)	3.42	3	2.8	2.8	2.6
Indirect band gap (eV)	2.7	2.4	2.4	2.2	2.1
Band tail (eV)	–	0.22	0.23	0.27	0.37

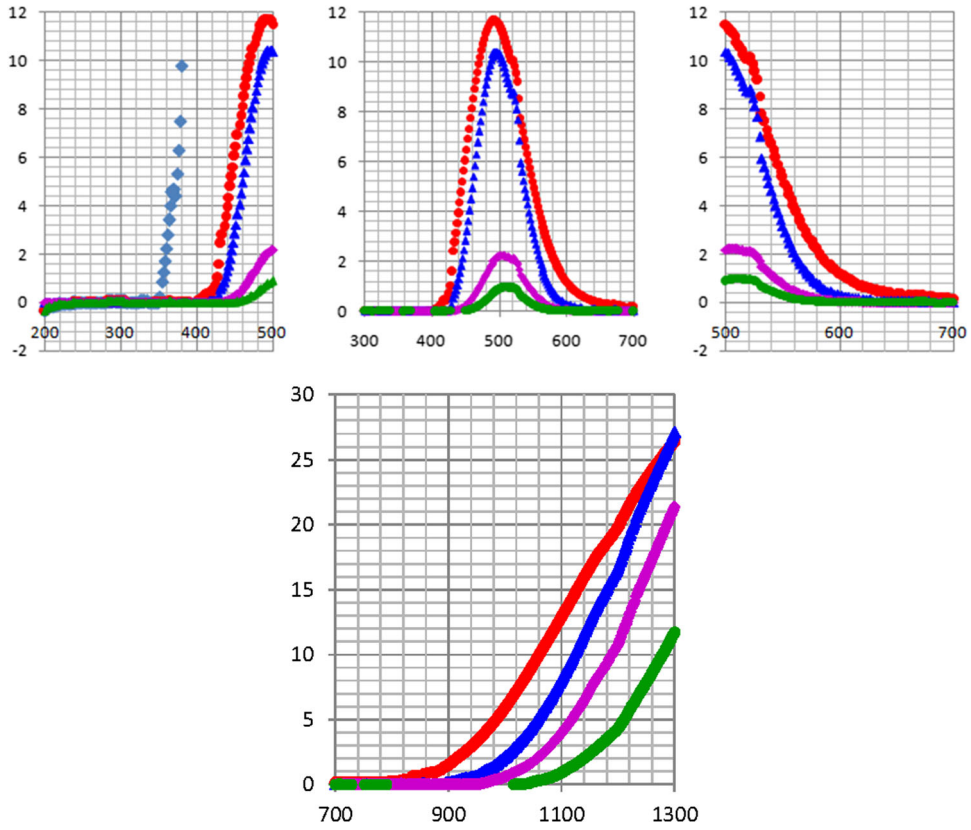

Fig. 10 Cutoff and bandstop filter of UV and IR

to 20 %. The IR cutoff and IR bandstop filter are shown in Fig. 10. The bandstop in the IR band begins with 800 nm and ends to 1060 nm.

The absorption broadband around 740 nm for all glass samples was observed which is due to Cu^{+2} in distorted octahedral group [23–25]. By the addition of copper content, the absorption peak shifts to high wavelength and increases the intensity up to 25 mol%. The observed shift to near-infrared region is due to the formation of copper tetrahedral group [24–26].

These observations indicate a gradual increase in the concentration of Cu^{2+} ions that take modifying positions in the glass network. This caused the higher content of NBOs in the glass matrix [5]. This leads to increase in the degree of localization of electrons, thereby increasing the donor centers in the glass matrix. This decreases the optical band gap.

In the present glass network, Cu^{2+} ion is considered to be in octahedral, tetragonal and square planar coordination. As the concentration of CuO is increased, an increase in the

intensity of the broadband is observed. Such an increase indicates the conversion of a part of Cu^{+} ions to Cu^{2+} ions. The highest intensity of these two kinds observed in the spectrum of glass containing 25 mol% CuO suggests the presence of larger concentration of Cu^{+} ions in this glass.

The absorption coefficient is related to photon energy by the relation [27]:

$$\alpha = A\left(h\nu - E_{\text{opt}}\right)^{n}/h\nu \quad (1)$$

where A is constant, E_{opt} is the energy gap and n is constant that depends on the mechanism of electron transition, wherein the direct transition, n, has (1/2 or 3/2) and indirect transition, n, has (2 or 3) depending on whether the transition is allowed or forbidden [28]. The value of E_{opt} and n can be determined by drawing a relation between $\alpha h\nu^{1/n}$ and $h\nu$.

The best fit was found to be with $n = 1/2$, which is the characteristic behavior of indirect transition in all studied samples. The relation between E_{opt} and CuO content is shown in Fig. 11. From Fig. 12, it can be seen that the optical gap decreases with the increase in copper content in glass samples.

The decrease in E_{opt} with increasing copper content in lead borate glass samples could be related to the change in bridging oxygen BO to non-bridging oxygen NBO (good agreement with results of infrared), which binds excited electrons less firmly than bridging oxygen [29]. The ultraviolet transparency of oxide glasses has been investigated in terms of electronegativity of the ingredient oxygen atoms [30]. In glasses, negative charge on the NBOs is larger than that on the bridging oxygen. Increasing the iconicity of oxygen ions by converting them from BO to NBO ions decreases the band gap energy E_{opt}. The concentration of NBOs in the glass matrix is higher [5]. This leads to increase in the degree of localization of electrons, thereby increasing the donor centers in the glass matrix. The presence of larger concentration of these donor centers decreases the optical band gap.

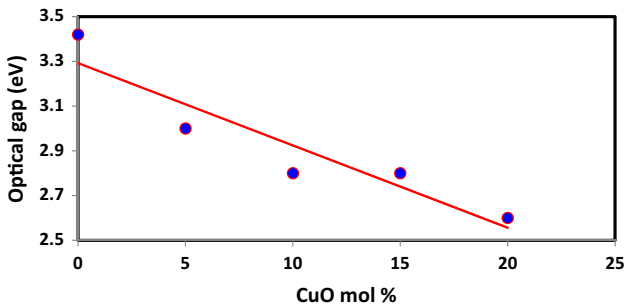

Fig. 11 Relation between optical energy gap and copper oxide content

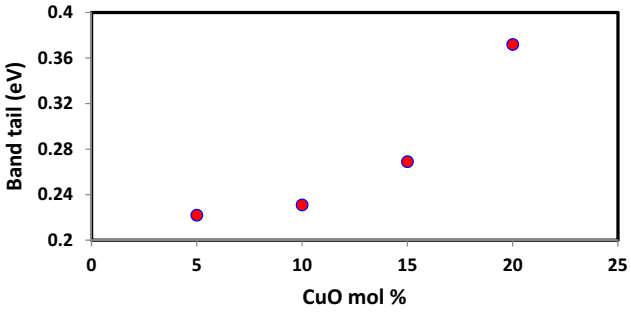

Fig. 12 Relation between Urbach energy Et and CuO content

The width of the band tail was calculated using Urbach's formula [31]

$$\ln\alpha = \ln B + (h\nu/\boldsymbol{E_t}) \quad (2)$$

where B is constant and $\boldsymbol{E_t}$ is the width of the tail (localized states) in the optical band gap.

Figure 12 shows the relation between Urbach energy $\boldsymbol{E_t}$ and CuO content. From Fig. 12, it can be observed that the Urbach energy $\boldsymbol{E_t}$ increases with the increase in the copper content. Urbach energy, which corresponds to the width of localized states, is used to characterize the degree of disorder in amorphous and crystalline systems. Materials with large Urbach energy would have greater tendency to convert weak bonds into defects. As a result, the defect concentration could be determined by the measure of Urbach energy.

The dielectric constant can be calculated according to the relations [32]

$$\acute{\varepsilon} = n^2 - k^2 \quad (3)$$

and

$$\varepsilon = 2nk \quad (4)$$

where n is the refractive index and k is the extinction coefficient and calculated according Eq. (5)

$$k = \alpha\lambda/4\pi \quad (5)$$

[α is the absorption coefficient and λ is the wavelength]

Figure 13a, b shows the relation between $\acute{\varepsilon}$ and ε as a function of wavelength.

As shown in Fig. 13a, b, the electrooptical phenomena at the same wavelength (start and end bandpass) can be observed [24]. Lithium lead borate glass samples containing copper oxide are used to remove a region of the near-infrared spectrum from sunlight and to produce glasses which transmit in the green region.

The ultraviolet cutoff wavelength of glass samples is shifted toward the visible region by the addition of copper oxides to lithium lead borate. The addition of copper oxide formed the non-bridging oxygen in the glass network,

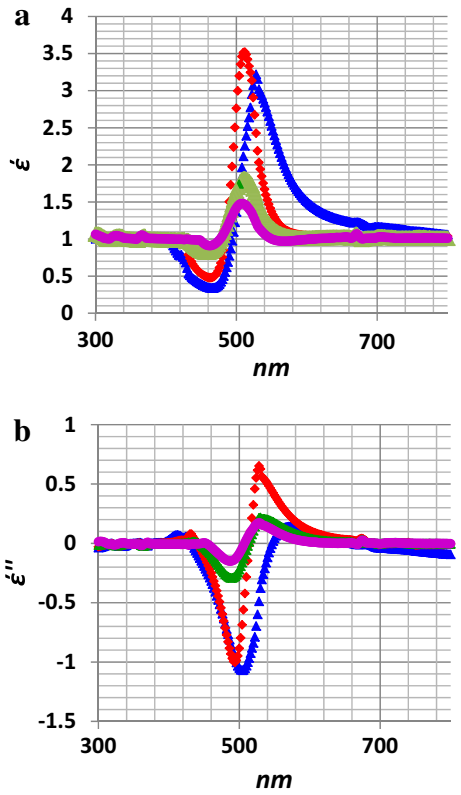

Fig. 13 **a**, **b** Relation between $\acute{\varepsilon}$ and ε as a function of wavelength

which shifts the ultraviolet cutoff toward the visible region, forms longpass glass filter with cutoff wavelengths which vary with the non-bridging oxygen concentration and creates charge transfer bands, producing longpass filters with cutoffs in the range of 190 to 400 nm.

4 Conclusion

The trends of densities, conductivities and magnetic susceptibility are attributed to changes in the glass network structure. This behavior can be attributed to the transformation of copper ions from network modifier positions to network former positions. The conduction mechanism was found due to ionic and electronic conduction. And the magnetic susceptibility χ depends on the change of the role of copper ions in the sample's structure due to the change in the copper glass-forming oxide. The optical properties indicate that the copper ions coexist in Cu^{+} state with Cu^{2+} state. The optical energy band gap E_{opt} increases and the Urbach energy E_{tail} decreases with the increase in the concentration of CuO up to 20 mol%. This leads to the increase in the degree of localization of electrons, thereby increasing the donor centers in the glass matrix. The glass samples containing copper are used as longpass filter and absorption glass.

References

1. M. Ganguli, K.J. Rao, J. Solid State Chem. **145**(1), 65–76 (1999)
2. I. Kashif, A.A. Soliman, H. Farouk, M. El-Shorpagy, A.M. Sanad, Physica B **403**(21), 3903–3906 (2008)
3. N.A. El-Alaily, R.M. Mohamed, Mater. Sci. Eng., B **98**(3), 193–203 (2003)
4. Y. Cheng, H. Xiao, W. Guo, Ceram. Int. **33**(7), 1341–1347 (2007)
5. I. Kashif, A. Abd El-ghany, A. Abd El-Maboud, M.A. Elsherbiny, A.M. Sanad, J. Alloys Compd. **503**(2), 384–388 (2010)
6. M. Prashant Kumar, T. Sankarappa, Materials Science-Poland, 26(3), 647–657 (2008)
7. F.H. ElBatal, S.Y. Marzouk, N. Nada, S.M. Desouky, Phys. B Condens. Matter. **391**(1), 88–97 (2007)
8. H. Farouk, Y.M. Abo-Zeid, M.A. Khaled, I. Kashif, A.M. Sanad, J. Mater. Sci.: Mater. Electron. **6**(6), 393–396 (1995)
9. B.V.R. Chowdari, K.L. Tan, W.T. Chia, R. Gopalakrishnan, J. Non Cryst. Solids **128**(1), 18–29 (1991)
10. P. Pascuta, L. Pop, S. Rada, M. Bosca, E. Culea, J. Mater. Sci.: Mater. Electron. **19**(5), 424–428 (2008)
11. R.P. Sreekanth Chakradhar, B. Yasoda, J. Lakshmana Rao, N.O. Gopal, J. Non Cryst. Solids **352**(36), 3864–3871 (2006)
12. Z.P. Lu, C.T. Liu, Acta Mater. **50**, 3501–3512 (2002)
13. I. Ardelean, M. Peteanu, R. Ciceo-Lucacel, I. Bratu, J. Mater. Sci.: Mater. Electron. **11**(1), 11–16 (2000)
14. Y. Cheng, H. Xiao, W. Guo, Ceram. Int. **34**(5), 1335–1339 (2008)
15. V. Ramesh Kumar, J.L. Rao, N.O. Gopal, Mater. Res. Bull. **40**(8), 1256–1269 (2005)
16. P.S. Gahlot, V.P. Seth, A. Agarwal, S. Sanghi, P. Chand, D.R. Goyal, Phys. B Condens. Matter. **355**(1–4), 44–53 (2005)
17. A.A. Soliman, E.M. Sakr, I. Kashif, Mater. Sci. Eng., B **158**, 30–34 (2009)
18. N.F. Mott, Philos. Mag. **19**(160), 835–852 (1969)
19. A. Latia, C. Vancea, J. Optoelectron. Adv. Mater. **5**(1), 185–190 (2003)
20. P.Y. Shih, S.W. Yung, T.S. Chin, J. Non Cryst. Solids **244**(2-3), 211–222 (1999)
21. E.E. Metwalli, J. Non Cryst. Solids **317**(3), 221–230 (2003)
22. G. Lakshminarayana, S. Buddhudu, Spectrochim. Acta Part A Mol. Biomol. Spectrosc. **62**(1–3), 364–371 (2005)
23. G.D. Khattak, A. Mekki, L.E. Wenger, J. Non-Cryst. Solids **337**(2), 174–181 (2004)
24. I. Kashif, A. Ratep, A.M. Sanad, Opt. Quant. Electron. **47**, 673–684 (2015)
25. B. Karthikeyan, Spectrochim. Acta A Mol. Biomol. Spectrosc. **66**, 860–862 (2007)
26. A.B.P. Lever, *Inorganic Electronic, Spectroscopy* (Elsevier, Amsterdam, 1968)
27. N.F. Mott, E.A. Davis, *Electronic Process in Non-crystalline Materials*, 1st edn. (Oxford University Press, Oxford, 1971)
28. N.V.V. Prasad, K. Annapurna, N.S. Hussain, S. Buddhudu, Mater. Lett. **57**, 2071–2080 (2003)
29. V.I. Arbuzov, Glass Phys. Chem. **22**, 477–489 (1996)
30. J.A. Duffy, Phys. Chem. Glasses **42**, 151–157 (2001)
31. A.K. Varshneya, *Fundamentals of Inorganic Glasses* (Academic press Inc., New York, 1994)
32. M.Y. Nadeem, W. Ahmed, Turk. J. Phys. **24**, 651–659 (2000)